Nonlinear Control of a Multirotor UAV with Suspended Load

Kristian Klausen*, Thor I. Fossen†, Tor Arne Johansen‡
Centre for Autonomous Marine Operations and Systems (AMOS)
Department of Engineering Cybernetics,
Norwegian University of Science and Technology (NTNU), 7491 Trondheim, Norway
Email: *kristian.klausen@ntnu.no, †thor.fossen@ntnu.no, ‡tor.arne.johansen@itk.ntnu.no

***Abstract*—This paper considers the control of a multirotor-type unmanned aerial vehicle (UAV) with a suspended load. The load is modeled as a pendulum, with a rigid link. We consider the case when the suspended load is connected to the centre of gravity of the UAV, and the interconnected system is modeled by Kane's method. A nonlinear controller based on the backstepping technique is derived, that ensures trajectory tracking of the UAV regardless of the pendulum motion. The origin of the tracking error is proved to be globally asymptotically stable, and results are verified by simulations.**

I. Introduction

The ability to remotely deploy sensors or other payload packages with unmanned aerial vehicles (UAVs), would enable several interesting applications. For instance, one could automatically deploy and recover environmental sensors in hazardous areas, or to areas that are hard or expensive to reach with traditional means. To this end, the use of multirotor type UAVs has several benefits. Several types of multi-rotor UAVs are available today, where the most common are the quadcopter. Multirotors are able to hover, which would enable gentle placement of the payload. They are also capable of maneuvering in complex environments.

Dynamic modeling and attitude control of the multirotor UAV itself have been extensively studied in the literature. This includes several nonlinear attitude controllers [1], [2], [3]. In [4], the authors give a good overview of the current state-of the art control techniques and dominant physical effects on the aerodynamics of the vehicles.

This work was partially supported by the Research Council of Norway through its Centers of Excellence funding scheme, grant number 223254 (Centre for Autonomous Marine Operations and Systems).

In this paper, we consider the transportation phase of a mission composed of a multirotor UAV, carrying a payload suspended by a wire. Previous work on this topic includes [2], were the authors employ an adaptive controller to respond to changes in the multirotor centre of gravity. In [5], the authors models the wire as a series of interconnected links, and develop a nonlinear geometric controller to stabilize the system. [6] models the multirotor-payload system with a hybrid approach to handle wire collapse, and develops trajectory controllers for the load position in 2D. Helicopters with suspended loads are considered in [7],[8], which also included multi-lift operations.

We develop a nonlinear tracking controller for a single-lift operation, where a single multirotor transports a suspended load with known mass. The proposed controller can later be extended to include systems with unknown load mass, and also for trajectory synchronization in multi-vehicle operations.

Although damping of the payload swing is not the focus of this paper, we illustrate how one classical approach, namely Input Shaping [9], can be used to generate trajectories that minimizes the residual swing of the suspended payload.

A. Organization

In Section II, we outline the basis for the mathematical models used for control synthesis. The interconnected model of the UAV and the suspended payload is based on Kane's equation. In Section III, we develop a nonlinear tracking controller based on the backstepping technique. The results are summarized in Theorem 1, and

proved by Lyapunov analysis. Two numerical simulations are conducted in Section IV, to show the performance of the controller.

II. System modeling

In this section, we start by presenting the dynamical model of a multirotor. The model (1)–(4) can be derived by Newtonian or Lagrangian methods, and readers are referred to [4] for details on its derivation. By further assuming the presence of an internal attitude controller, the relevant dynamics for this study is extracted. Finally, the dynamics of the complete system including the suspended load are introduced.

Let the multirotor dynamics be modeled by [4]

$$\dot{\mathbf{p}} = \mathbf{v} \tag{1}$$
$$m_c\dot{\mathbf{v}} = m_c\mathbf{g} + \mathbf{R}f \tag{2}$$
$$\dot{\mathbf{R}} = \mathbf{R}\mathbf{S}(\omega) \tag{3}$$
$$I\dot{\omega} = \mathbf{S}(I\omega)\omega + \mathbf{M} \tag{4}$$

where $\mathbf{p} \in \mathbb{R}^3$ is the UAV position in the inertial frame $\{n\}$, $\mathbf{v} \in \mathbb{R}^3$ the translational velocity in $\{n\}$, $\mathbf{R} \in \mathcal{SO}^3$ a rotation matrix from the inertial frame $\{n\}$ to the body-fixed frame $\{b\}$, $\omega \in \mathbb{R}^3$ the angular velocity of the UAV, represented in $\{b\}$. Further, the operator $\mathbf{S}(\cdot)$ is the skew-symmetric transformation, such that $p \times q = \mathbf{S}(p)q$. m_c is the mass of the UAV, and I the body-fixed inertia matrix. f is upwards thrust directed along the negative body-aligned z-axis, and $\mathbf{M}$ are applied moment about the UAV.

Consider now a load being suspended in the centre of gravity of the UAV. This will affect the translational motion (2) by a term τ_L, parameterized by the load dynamics, but the rotational motion (4) is unaffected. As control of the attitude of the multicopter is not considered in this paper, the model considering the translational motion is now

$$\dot{\mathbf{p}} = \mathbf{v} \tag{5}$$
$$m_c\dot{\mathbf{v}} = m_c\mathbf{g} + \mathbf{R}f + \tau_L \tag{6}$$

Further, assume now that a sufficiently fast attitude controller is present. The direction of the applied force for translational motion is given by $\mathbf{R}$, and by manipulating the roll and pitch of the UAV we can apply force in a desired direction. An example of such a controller is given in [4]. Thus, the term $\mathbf{R}f$ can be replaced by a inertial control force $\mathbf{F} \in \mathbb{R}^3$, resulting in

$$\dot{\mathbf{p}} = \mathbf{v} \tag{7}$$
$$m_c\dot{\mathbf{v}} = m_c\mathbf{g} + \mathbf{F} + \tau_L \tag{8}$$

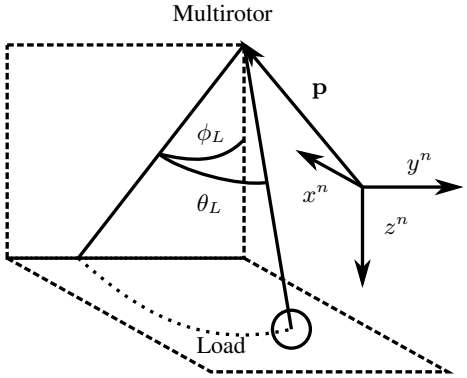

Fig. 1. Illustration of pendulum angle parameterization by two consecutive rotations ϕ_L and θ_L about the x- and y-axis, respectively.

Next, the suspended load dynamics are modeled as a pendulum. This simple model have been used with success in earlier work [10]. We consider the suspended load a point-mass, connected by a rigid link to the centre of gravity of the UAV. This is valid for non-aggressive maneuvers where the wire remains in tension. We parameterize the pendulum displacements by ϕ_L and θ_L, which is the load rotation about the inertial x- and y-axis, respectively, see Figure 1. The generalized coordinates for the system are thus $\boldsymbol{\eta} = [\mathbf{p}, \phi_L, \theta_L]$. Physical damping of the pendulum swing is modeled by a linear damping term, which is valid for low speeds. By utilizing Kane's equation [11], we get the dynamical model given by (9):

$$\begin{aligned} \dot{\boldsymbol{\eta}} &= \boldsymbol{\nu} \\ \mathbf{M}^*(\boldsymbol{\eta})\dot{\boldsymbol{\nu}} + \mathbf{C}^*(\boldsymbol{\eta},\boldsymbol{\nu})\boldsymbol{\nu} + \mathbf{G}(\boldsymbol{\eta}) + \mathbf{D}\boldsymbol{\nu} &= \boldsymbol{\tau} \end{aligned} \tag{9}$$

where $\mathbf{M}^*(\boldsymbol{\eta})$ and $\mathbf{C}^*(\boldsymbol{\eta},\boldsymbol{\nu})$ can be seen in (10)–(11), $\boldsymbol{\tau} := \begin{bmatrix}\mathbf{F} & \mathbf{0}_{1\times 2}\end{bmatrix}^{\mathrm{T}}$, $\boldsymbol{\nu} := [\mathbf{v}^{\mathrm{T}}, \dot{\phi}_L, \dot{\theta}_L]^{\mathrm{T}}$, and

$$\mathbf{M}^*(\boldsymbol{\eta}) = \begin{bmatrix} m_L + m_c & 0 & 0 & 0 & L\,m_L\,\mathrm{c}\theta_L \\ 0 & m_L + m_c & 0 & -L\,m_L\,\mathrm{c}\phi_L\,\mathrm{c}\theta_L & L\,m_L\,\mathrm{s}\phi_L\,\mathrm{s}\theta_L \\ 0 & 0 & m_L + m_c & -L\,m_L\,\mathrm{c}\theta_L\,\mathrm{s}\phi_L & -L\,m_L\,\mathrm{c}\phi_L\,\mathrm{s}\theta_L \\ 0 & -L\,m_L\,\mathrm{c}\phi_L\,\mathrm{c}\theta_L & -L\,m_L\,\mathrm{c}\theta_L\,\mathrm{s}\phi_L & L^2\,m_L\,\mathrm{c}{\theta_L}^2 & 0 \\ L\,m_L\,\mathrm{c}\theta_L & L\,m_L\,\mathrm{s}\phi_L\,\mathrm{s}\theta_L & -L\,m_L\,\mathrm{c}\phi_L\,\mathrm{s}\theta_L & 0 & L^2\,m_L \end{bmatrix} \tag{10}$$

$$\mathbf{C}^*(\boldsymbol{\eta},\boldsymbol{\nu}) = \begin{bmatrix} 0 & 0 & 0 & 0 & -L\,\dot{\theta}_L\,m_L\,\mathrm{s}\theta_L \\ 0 & 0 & 0 & L\,m_L\left(\dot{\phi}_L\,\mathrm{c}\theta_L\,\mathrm{s}\phi_L + \dot{\theta}_L\,\mathrm{c}\phi_L\,\mathrm{s}\theta_L\right) & L\,m_L\left(\dot{\phi}_L\,\mathrm{c}\phi_L\,\mathrm{s}\theta_L + \dot{\theta}_L\,\mathrm{c}\theta_L\,\mathrm{s}\phi_L\right) \\ 0 & 0 & 0 & -L\,m_L\left(\dot{\phi}_L\,\mathrm{c}\phi_L\,\mathrm{c}\theta_L - \dot{\theta}_L\,\mathrm{s}\phi_L\,\mathrm{s}\theta_L\right) & -L\,m_L\left(\dot{\theta}_L\,\mathrm{c}\phi_L\,\mathrm{c}\theta_L - \dot{\phi}_L\,\mathrm{s}\phi_L\,\mathrm{s}\theta_L\right) \\ 0 & 0 & 0 & -\frac{1}{2}L^2\,\dot{\theta}_L\,m_L\,\mathrm{s}(2\,\theta_L) & -\frac{1}{2}L^2\,\dot{\phi}_L\,m_L\,\mathrm{s}(2\,\theta_L) \\ 0 & 0 & 0 & \frac{1}{2}L^2\,\dot{\phi}_L\,m_L\,\mathrm{s}(2\,\theta_L) & 0 \end{bmatrix} \tag{11}$$

$$\mathbf{G}(\boldsymbol{\eta}) = \begin{bmatrix} 0 \\ 0 \\ -g\ (m_L + m_c) \\ L\,g\,m_L\ \cos\theta_L\ \sin\phi_L \\ L\,g\,m_L\ \cos\phi_L\ \sin\theta_L \end{bmatrix}. \tag{12}$$

The term $\mathbf{D}\boldsymbol{\nu}$ is the linear damping force, incorporating the effects of air drag at low speed. $\mathbf{D} = \mathtt{diag}\{[0,0,0,d,d]\}$, where $d > 0$ is a drag coefficient.

As can be seen in (9), the equations are organized in matrix form, which is typical in the literature of robotic manipulation. This form greatly simplifies the control and analysis procedures. In fact, as is common in robotic manipulators, the matrix $\dot{\mathbf{M}}^*(\boldsymbol{\eta}) - 2\mathbf{C}^*(\boldsymbol{\eta},\boldsymbol{\nu})$ is skew symmetric, which is a very useful property in Lyapunov analysis. As can be seen from (10), $\mathbf{M}^*(\boldsymbol{\eta})$ is singular at $\theta_L = \pi/2$. This is due to the representation of the pendulum configuration, and corresponds to the case where the suspended load is directed out of the nose of the UAV. Although this may violate the assumptions of pendulum model and load being suspended on CG, we illustrate in the next section how a infinitesimal *singularity avoidance* term can be added to use the model for theoretically valid control design and analysis.

III. Control Design

In this section, we design a nonlinear trajectory-tracking controller for the UAV. We utilize the backstepping technique [12], to design the controllers in two steps. To achieve this, with a slight abuse of terminology, we view (9) as an under actuated system, in which element 4 and 5 of $\boldsymbol{\tau}$ is zero. The design procedure is inspired by [13]

The model developed in the previous section has a representation singularity at $\theta_L = \pi/2$. This is an undesired feature in control-design. Thus, we create a perturbed model, in which we avoid the singularity by adding an infinitesimal *singularity avoidance* term at $\mathbf{M}^*_{4,4}$. The model used for control design are then:

$$\dot{\boldsymbol{\eta}} = \boldsymbol{\nu} \tag{13}$$

$$\mathbf{M}(\boldsymbol{\eta})\dot{\boldsymbol{\nu}} + \mathbf{C}(\boldsymbol{\eta},\boldsymbol{\nu})\boldsymbol{\nu} + \mathbf{G}(\boldsymbol{\eta}) + \mathbf{D}\boldsymbol{\nu} = \boldsymbol{\tau} \tag{14}$$

where $\mathbf{M}(\boldsymbol{\eta}) = \mathbf{M}^*(\boldsymbol{\eta})$, $\mathbf{C}(\boldsymbol{\eta},\boldsymbol{\nu}) = \mathbf{C}^*(\boldsymbol{\eta},\boldsymbol{\nu})$ except for

$$\mathbf{M}(\boldsymbol{\eta})_{4,4} = L^2 m_L \cos{\theta_L}^2 + \varepsilon \sin{\theta_L}^2, \tag{15}$$

and

$$\mathbf{C}(\boldsymbol{\eta},\boldsymbol{\nu})_{4,4} = -\frac{1}{2}L^2 m_L \dot{\theta}_L \sin 2\theta_L + \frac{1}{2}\varepsilon\dot{\theta}_L \sin 2\theta_L. \tag{16}$$

$\varepsilon > 0$ is an infinitesimal positive constant. As can be seen, $\mathbf{C}(\boldsymbol{\eta},\boldsymbol{\nu})$ is also perturbed to maintain the skew-symetric property. This added term ensures that the mass matrix is non-singular. This perturbed model is now used in the rest of this section.

Consider now a sufficiently smooth desired trajectory $\mathbf{r}(t)$. We define the error signals $\mathbf{z}_1 \in \mathbb{R}^3$ and $\mathbf{z}_2 \in \mathbb{R}^5$ as

$$\mathbf{z}_1 := \mathbf{p} - \mathbf{r} \tag{17}$$

$$\mathbf{z}_2 := \left[z_{2,1}, z_{2,2}, z_{2,3}, z_{2,4}, z_{2,5}\right]^{\mathrm{T}} = \boldsymbol{\nu} - \boldsymbol{\alpha} \tag{18}$$

where $\boldsymbol{\alpha} := [\alpha_1, \alpha_2, \alpha_3, \alpha_4, \alpha_5]^{\mathrm{T}} \in \mathbb{R}^5$ is a vector of stabilizing functions to be specified later.

Now, let $\mathbf{H}$ be the selection matrix

$$\mathbf{H} = \begin{bmatrix} 1 & 0 & 0 & 0 & 0 \\ 0 & 1 & 0 & 0 & 0 \\ 0 & 0 & 1 & 0 & 0 \end{bmatrix} \tag{19}$$

such that error dynamics becomes

$$\dot{\mathbf{z}}_1 = \mathbf{H}\boldsymbol{\nu} - \dot{\mathbf{r}} \tag{20}$$

and

$$\begin{aligned} \mathbf{M}(\boldsymbol{\eta})\dot{\mathbf{z}}_2 &= \mathbf{M}(\boldsymbol{\eta})\dot{\boldsymbol{\nu}} - \mathbf{M}(\boldsymbol{\eta})\dot{\boldsymbol{\alpha}} \\ &= \boldsymbol{\tau} - \mathbf{C}(\boldsymbol{\eta}, \boldsymbol{\nu})\boldsymbol{\nu} - \mathbf{G}(\boldsymbol{\eta}) \\ &\quad - \mathbf{D}\boldsymbol{\nu} - \mathbf{M}(\boldsymbol{\eta})\dot{\boldsymbol{\alpha}} \end{aligned} \tag{21}$$

A. Step I

Consider a Lyapunov function candidate (LFC) for the first sub-system as

$$V_1(\mathbf{z}_1, t) = \frac{1}{2}\mathbf{z}_1^{\mathrm{T}}\mathbf{z}_1 \tag{22}$$

It's derivative along the solution of $\mathbf{z}_1(t)$ is

$$\begin{aligned} \dot{V}_1(\mathbf{z}_1, t) &= \mathbf{z}_1^{\mathrm{T}}(\mathbf{H}\boldsymbol{\nu} - \dot{\mathbf{r}}) \\ &= \mathbf{z}_1^{\mathrm{T}}(\boldsymbol{\alpha}_{1:3} + \mathbf{H}\mathbf{z}_2 - \dot{\mathbf{r}}) \end{aligned} \tag{23}$$

where $(\cdot)_{i:j}$ represents the 1-indexed elements of $(\cdot)$ from i to j. By designing the stabilizing functions $\boldsymbol{\alpha}_{1:3}$ as

$$\boldsymbol{\alpha}_{1:3} = \dot{\mathbf{r}} - \mathbf{K}_1\mathbf{z}_1, \tag{24}$$

where $\mathbf{K}_1 = \mathbf{K}_1^{\mathrm{T}} > 0$ is a positive definite matrix. The derivative of $V_1(\mathbf{z}_1, t)$ becomes

$$\dot{V}_1(\mathbf{z}_1, t) = -\mathbf{z}_1^{\mathrm{T}}\mathbf{K}_1\mathbf{z}_1 + \mathbf{z}_1^{\mathrm{T}}\mathbf{H}\mathbf{z}_2 \tag{25}$$

B. Step II

Next, consider the LFC $V_2(\mathbf{z}_1, \mathbf{z}_2, t)$ for the complete system as:

$$V_2(\mathbf{z}_1, \mathbf{z}_2, t) = V_1(\mathbf{z}_1, t) + \frac{1}{2}\mathbf{z}_2^{\mathrm{T}}\mathbf{M}(\boldsymbol{\eta})\mathbf{z}_2 \tag{26}$$

which satisfies

$$V_2 \geq 0, \ \forall(\mathbf{z}_1, \mathbf{z}_2) \neq 0 \tag{27}$$

Taking the derivative of (26) along the solution of (20) and (21) yields

$$\begin{aligned} \dot{V}_2(\mathbf{z}_1, \mathbf{z}_2, t) &= -\mathbf{z}_1^{\mathrm{T}}\mathbf{K}_1\mathbf{z}_1 \\ &\quad + \mathbf{z}_2^{\mathrm{T}}(\boldsymbol{\tau} - \mathbf{C}\boldsymbol{\alpha} - \mathbf{G} - \mathbf{D}\boldsymbol{\nu} + \mathbf{H}^{\mathrm{T}}\mathbf{z}_1 - \mathbf{M}\dot{\boldsymbol{\alpha}}) \end{aligned}$$

where we have utilized the skew-symetric property of $\frac{1}{2}\dot{\mathbf{M}}(\boldsymbol{\eta}) - \mathbf{C}(\boldsymbol{\eta}, \boldsymbol{\nu})$. Suppose now that the control $\boldsymbol{\tau}$ can be set to

$$\boldsymbol{\tau} = \mathbf{C}\boldsymbol{\alpha} + \mathbf{G} + \mathbf{D}\boldsymbol{\alpha} - \mathbf{H}^{\mathrm{T}}\mathbf{z}_1 + \mathbf{M}\dot{\boldsymbol{\alpha}} - \mathbf{K}_2\mathbf{z}_2 \tag{28}$$

where $\mathbf{K}_2 = \mathbf{K}_2^{\mathrm{T}} > 0$. This results in

$$\begin{aligned} \dot{V}_2(\mathbf{z}_1, \mathbf{z}_2, t) &= -\mathbf{z}_1^{\mathrm{T}}\mathbf{K}_1\mathbf{z}_1 - \mathbf{z}_2^{\mathrm{T}}\mathbf{K}_2\mathbf{z}_2 - \mathbf{z}_2^{\mathrm{T}}\mathbf{D}\mathbf{z}_2 \\ &< 0, \ \ \forall(\mathbf{z}_1, \mathbf{z}_2) \neq 0 \end{aligned}$$

which by standard Lyapunov arguments guarantees that $(\mathbf{z}_1, \mathbf{z}_2)$ is bounded and converges to zero. However, as we cannot set a desired moment about the suspension point of the load, the fourth and fifth row of (28) must instead be equal to zero. We now design the remaining stabilizing functions α_4 and α_5 to ensure that the fourth and fifth row of (28) is indeed zero. By extracting these rows from (28), we get the constraint equations

$$\begin{aligned} \boldsymbol{\tau}_{4:5} = \begin{bmatrix} 0 \\ 0 \end{bmatrix} &= \mathbf{C}_{4:5;4:5}\boldsymbol{\alpha}_{4:5} + \mathbf{G}_{4:5} + \mathbf{D}_{4:5;4:5}\boldsymbol{\alpha}_{4:5} \\ &\quad + \mathbf{M}_{4:5;4:5}\dot{\boldsymbol{\alpha}}_{4:5} + \mathbf{M}_{4:5,1:3}\dot{\boldsymbol{\alpha}}_{1:3} - \mathbf{K}_{2,4:5}\mathbf{z}_{2,4:5} \end{aligned}$$

where the arguments of $\mathbf{C}$ and $\mathbf{M}$ have been dropped for notational clarity, and $(\cdot)_{i:j;k:l}$ extracts rows $i-j$, columns $k-l$ of $(\cdot)$ Solving for $\dot{\boldsymbol{\alpha}}_{4:5}$, this results in a dynamic equality constraint

$$\begin{aligned} \mathbf{M}_{\alpha}(\boldsymbol{\eta})\dot{\boldsymbol{\alpha}}_{4:5} = -\mathbf{D}_{\alpha}\boldsymbol{\alpha}_{4:5} - \mathbf{C}_{\alpha}(\boldsymbol{\eta}, \boldsymbol{\nu})\boldsymbol{\alpha}_{4:5} \\ + \boldsymbol{\gamma}(\boldsymbol{\eta}, \mathbf{z}_1, \mathbf{z}_2, \ddot{\mathbf{r}}) \end{aligned} \tag{29}$$

where

$$\begin{aligned}\mathbf{M}_\alpha(\boldsymbol{\eta}) &= \mathbf{M}_{4:5;4:5}(\boldsymbol{\eta}),\\ &\quad \text{the lower 2x2 block of } \mathbf{M}(\boldsymbol{\eta})\\ \mathbf{C}_\alpha(\boldsymbol{\eta},\boldsymbol{\nu}) &= \mathbf{C}_{4:5;4:5}(\boldsymbol{\eta},\boldsymbol{\nu}),\\ &\quad \text{the lower 2x2 block of } \mathbf{C}(\boldsymbol{\eta},\boldsymbol{\nu})\\ \mathbf{D}_\alpha &= \mathtt{diag}\{[d,d]\} > 0\end{aligned}$$

and

$$\begin{aligned}\boldsymbol{\gamma}(\boldsymbol{\eta},\mathbf{z}_1,\mathbf{z}_2,\ddot{\mathbf{r}}) &= -\mathbf{G}_{4:5} + \mathbf{K}_{2,4:5}\mathbf{z}_{2,4:5}\\ &\quad -\mathbf{M}_{4:5,1:3}(\ddot{\mathbf{r}} - \mathbf{K}_1\mathbf{H}\mathbf{z}_2 + \mathbf{K}_1\mathbf{K}_1\mathbf{z}_1)\end{aligned}$$

in which we have used the fact that

$$\begin{aligned}\dot{\boldsymbol{\alpha}}_{1:3} &= \ddot{\mathbf{r}} - \mathbf{K}_1\dot{\mathbf{z}}_1\\ &= \ddot{\mathbf{r}} - \mathbf{K}_1\mathbf{H}\mathbf{z}_2 + \mathbf{K}_1\mathbf{K}_1\mathbf{z}_1\end{aligned} \tag{30}$$

Also, note that the matrix $\dot{\mathbf{M}}_\alpha - 2\mathbf{C}_\alpha$ retains the skew-symetric property. The variables $\boldsymbol{\alpha}_{4:5}$ becomes a dynamic state in the controller, according to (29). In fact, (29) is a stable differential equation driven by the converging error signals $(\mathbf{z}_1,\mathbf{z}_2)$ and the bounded reference signal $\mathbf{r}$. As $\mathbf{z}_{2,4:5}(t)\to 0$, it follows that $|\boldsymbol{\alpha}_{4:5} - [\dot{\phi}_L,\dot{\theta}_L]^{\mathrm{T}}| \to 0$ as $t\to\infty$. This is stated more formally in Theorem 1.

Theorem 1. *The trajectory tracking problem of a multirotor UAV is solved by applying the first three rows of the control law* (28) *to* (14)*. Moreover,*

$$\begin{aligned}\mathbf{F} &= \mathbf{C}_{1:3;4:5}(\boldsymbol{\eta},\boldsymbol{\nu})\boldsymbol{\alpha}_{4:5} + \mathbf{G}_{1:3} - \mathbf{z}_1\\ &\quad + \mathbf{M}_{1:3;4:5}(\ddot{\mathbf{r}} - \mathbf{K}_1\mathbf{H}\mathbf{z}_2 + \mathbf{K}_1\mathbf{K}_1\mathbf{z}_1)\\ &\quad + \mathbf{M}_{1:3;4:5}\dot{\boldsymbol{\alpha}}_{4:5} - \mathbf{K}_{2,1:3}\mathbf{z}_{2,1:3}\end{aligned} \tag{31}$$

where $\mathbf{K}_1 > 0 \in \mathbb{R}^3$*,* $\mathbf{K}_2 > 0 \in \mathbb{R}^5$*,* $\mathbf{z}_1 := \mathbf{p} - \mathbf{r}$*,* $\mathbf{z}_2 := \boldsymbol{\nu} - \boldsymbol{\alpha}$*, and*

$$\boldsymbol{\alpha}_{1:3} = \dot{\mathbf{r}} - \mathbf{z}_1 \tag{32}$$

The smooth reference signals $\mathbf{r}$*,* $\dot{\mathbf{r}}$ *and* $\ddot{\mathbf{r}}$ *are provided by an external guidance system or a reference model, while* $\boldsymbol{\alpha}_{4:5}$ *are given by the dynamic constraint*

$$\begin{aligned}\mathbf{M}_\alpha(\boldsymbol{\eta})\dot{\boldsymbol{\alpha}}_{4:5} &= -\mathbf{D}_\alpha\boldsymbol{\alpha}_{4:5} - \mathbf{C}_\alpha(\boldsymbol{\eta},\boldsymbol{\nu})\boldsymbol{\alpha}_{4:5}\\ &\quad +\boldsymbol{\gamma}(\boldsymbol{\eta},\mathbf{z}_1,\mathbf{z}_2,\ddot{\mathbf{r}})\end{aligned} \tag{33}$$

The equilibrium point $(\mathbf{z}_1,\mathbf{z}_2) = 0$ *is Uniformally Globally Asymptotically Stable (UGAS),* $\boldsymbol{\alpha}_{4:5} \in \mathcal{L}_\infty$ *and satisfies*

$$\lim_{t\to\infty} |\boldsymbol{\alpha}_{4:5}(t) - [\dot{\phi}_L(t),\dot{\theta}_L(t)]^{\mathrm{T}}| = 0 \tag{34}$$

The control law (28) *thus guarantees that the tracking error* $\mathbf{z}_1 = \mathbf{p} - \mathbf{r}$ *converges asymptotically to zero.*

Proof. The closed-loop system can be expressed as

$$\begin{aligned}\begin{bmatrix}\mathbf{I}_{3\times3} & 0\\ 0 & \mathbf{M}(\boldsymbol{\eta})\end{bmatrix}\begin{bmatrix}\dot{\mathbf{z}}_1\\ \dot{\mathbf{z}}_2\end{bmatrix} &= \begin{bmatrix}-\mathbf{K}_1 & \mathbf{H}\\ -\mathbf{H}^{\mathrm{T}} & -\mathbf{D}-\mathbf{K}_2\end{bmatrix}\begin{bmatrix}\mathbf{z}_1\\ \mathbf{z}_2\end{bmatrix}\\ &\quad + \begin{bmatrix}\mathbf{0} & \mathbf{0}\\ \mathbf{0} & -\mathbf{C}(\boldsymbol{\eta},\boldsymbol{\nu})\end{bmatrix}\begin{bmatrix}\mathbf{z}_1\\ \mathbf{z}_2\end{bmatrix}\end{aligned} \tag{35}$$

$$\begin{aligned}\mathbf{M}_\alpha(\boldsymbol{\eta})\dot{\boldsymbol{\alpha}}_{4:5} &= -\mathbf{D}_\alpha\boldsymbol{\alpha}_{4:5} - \mathbf{C}_\alpha(\boldsymbol{\eta},\boldsymbol{\nu})\boldsymbol{\alpha}_{4:5}\\ &\quad +\boldsymbol{\gamma}(\boldsymbol{\eta},\mathbf{z}_1,\mathbf{z}_2,\ddot{\mathbf{r}})\end{aligned} \tag{36}$$

The Lyapunov function candidate (26) satisfies $\dot{V}_2 < 0, \forall(\mathbf{z}_1,\mathbf{z}_2) \neq 0$. Hence, the equilibrium point $\mathbf{z}_1 = \mathbf{z}_2 = 0$ of the $\mathbf{z}$ subsystem is UGAS [12, Theorem 4.9]. The unforced $\boldsymbol{\alpha}_{4:5}$ system, (29) with $\boldsymbol{\gamma} = 0$, is globally exponentially stable. This can be seen from the Lyapunov function

$$V_\alpha(\boldsymbol{\alpha}_{4:5},t) = \frac{1}{2}\boldsymbol{\alpha}_{4:5}^{\mathrm{T}}\mathbf{M}_\alpha(\boldsymbol{\eta})\boldsymbol{\alpha}_{4:5} \tag{37}$$

whos derivative along (29) is

$$\begin{aligned}\dot{V}_\alpha(\boldsymbol{\alpha}_{4:5},t) &= \boldsymbol{\alpha}_{4:5}^{\mathrm{T}}(-\mathbf{D}_\alpha\boldsymbol{\alpha}_{4:5} + \boldsymbol{\gamma})\\ &\leq -\frac{1}{2}\boldsymbol{\alpha}_{4:5}^{\mathrm{T}}\mathbf{D}_\alpha\boldsymbol{\alpha}_{4:5} \leq 0\end{aligned}$$

for $||\boldsymbol{\alpha}_{4:5}||_2 > 2||\boldsymbol{\gamma}||_2/d$. Since $(\mathbf{z}_1,\mathbf{z}_2) \in \mathcal{L}_\infty$, $\mathbf{r},\dot{\mathbf{r}},\ddot{\mathbf{r}} \in \mathcal{L}_\infty$ and since $\boldsymbol{\eta}$ enters $\boldsymbol{\gamma}$ through the bounded functions $\cos\cdot$ and $\sin\cdot$, we have $\boldsymbol{\gamma}(\boldsymbol{\eta},\mathbf{z}_1,\mathbf{z}_2,\ddot{\mathbf{r}}) \in \mathcal{L}_\infty$. Thus, the $\boldsymbol{\alpha}_{4:5}$ subsystem is input-to-state stable from $\boldsymbol{\gamma}$ to $\boldsymbol{\alpha}_{4:5}$ by [12, Theorem 4.19]. Hence, $\boldsymbol{\alpha}_{4:5}$ converges to the bounded set $\{\boldsymbol{\alpha}_{4:5} : ||\boldsymbol{\alpha}_{4:5}|| \leq \frac{2}{d}||\boldsymbol{\gamma}||\}$ since $\mathbf{z}_{2,4:5}(t)\to 0$ as $t\to\infty$. □

Remark 1. *Note that the global results presented in Theorem 1 applies to the perturbed model* (14)*. This model is valid as long as the wire is taut, and we stay somewhat away from the representation singularity at* $\theta_L = \pi/2$*. At this point, the model is perturbed by the infinitesimal constant* ε*, which in practice will have negligible impact on the results.*

Remark 2. *Also, note that the load angles* ϕ_L *and* θ_L *are not included in the coordinate change* (17)–(18)*, but their derivatives are. The angles acts as*

external inputs to the system dynamics through the saturating geometric functions cos *and* sin*, and are thus treated as bounded inputs in the analysis. See Figure 2.*

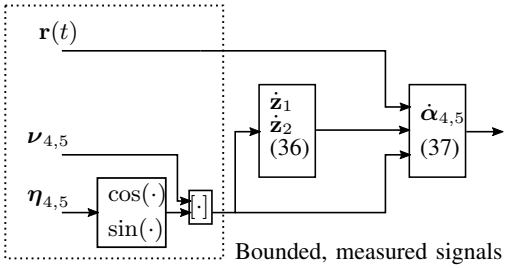

Fig. 2. Structure illustrating the proof. By Theorem 1, the feedback law (31) renders the origin of $[\mathbf{z}_1, \mathbf{z}_2]$ globally asymptotically stable. The signal $\boldsymbol{\alpha}_{4,5}$, needed by (31), is shown to be bounded. The load angles act on both sub-systems through the saturating trigonometric geometric functions $\cos(\cdot)$ and $\sin(\cdot)$, and $\boldsymbol{\nu}_{4,5}$ is bounded by (34).

IV. Simulation Study

In this section, the multi-rotor translational dynamics is simulated using (14), and the controller in Theorem 1 is used for trajectory control. We consider a multirotor of mass $m_c = 2.5$ kg, a payload of $m_L = 0.2$ kg suspended with a $L = 0.7$ m wire. Two simulations will be presented. The first will demonstrate the tracking capabilities of the controller in a complicated maneuver, while the second will supplement the controller with a trajectory generator that suppresses residual swings in the payload.

A. Trajectory Tracking

In this simulation, the multirotor will track a spiral-like trajectory, and come to a stop at the top of the spiral. The trajectory is fed through a third order reference model to generate the necessary signals $\mathbf{r}(t), \dot{\mathbf{r}}(t)$ and $\ddot{\mathbf{r}}(t)$, as illustrated in Figure 3. The reference model is given by (38), where $\omega_0 = 2$, $\zeta = 1/\sqrt{2}$ are tuning parameters, and we can acquire the reference signals by $[\mathbf{r}(t), \dot{\mathbf{r}}(t), \ddot{\mathbf{r}}(t)] = \boldsymbol{\xi}(t) \in \mathbb{R}^9$. The resulting trajectory $\mathbf{r}(t)$ can be seen in Figure 4.

The system is simulated in Matlab, and (14) is solved using the RK4 method at 100 Hz. In Figure 5 the actual multirotor position vs desired position is shown, and we see that the controller is capable of tracking the reference signal completely.

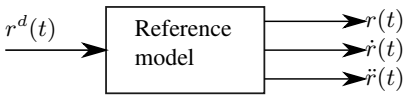

Fig. 3. Trajectory generation structure with a third-order reference model.

This is in spite of the heavy movement of the suspended payload, as can be seen in Figure 6. Note that in practice, the model is not valid for such high load swing angles, but the results illustrate the capabilities of the controller non the less. In practice, additional filters needs to be added to reduce the induced swing the payload. The procedure is illustrated in the next section.

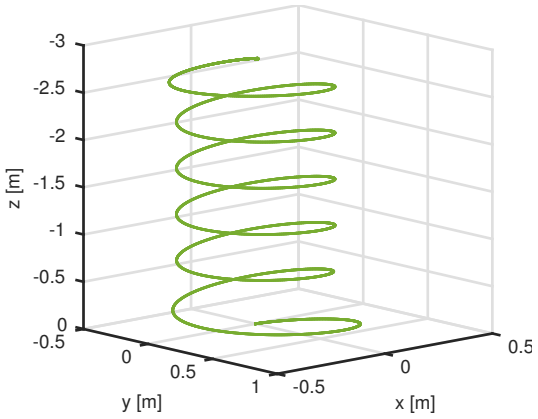

Fig. 4. Spiral reference-path in the first simulation.

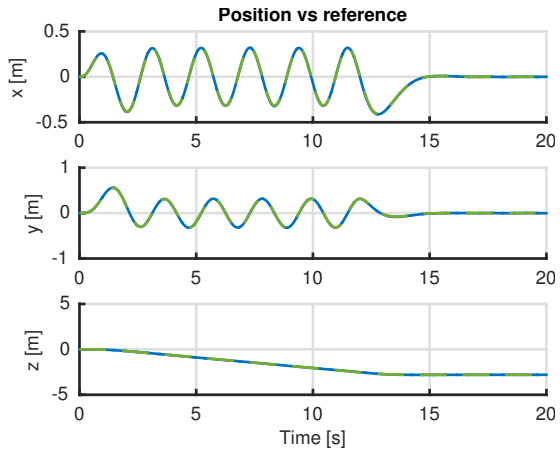

Fig. 5. Multi-rotor position (blue) vs reference trajectory (dashed green).

B. Swing-free maneuver

In this simulation, we utilize a method called Input-Shape Filtering to generate a reference trajectory that minimizes the residual swing in the

$$\dot{\boldsymbol{\xi}} = \begin{bmatrix} 0 & \mathbf{1}_{3\times3} & 0 \\ 0 & 0 & \mathbf{1}_{3\times3} \\ -\omega_0^3\mathbf{1}_{3\times3} & -(2\zeta+1)\omega_0^2\mathbf{1}_{3\times3} & -(2\zeta+1)\omega_0\mathbf{1}_{3\times3} \end{bmatrix} \boldsymbol{\xi} + \begin{bmatrix} \mathbf{1}_{3\times3} \\ 0 \\ 0 \end{bmatrix} \mathbf{r}^d \tag{38}$$

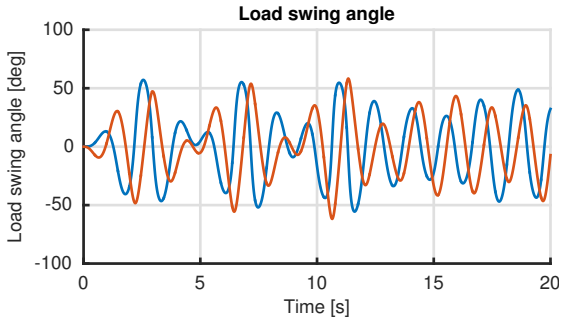

Fig. 6. Load swing-angles during first simulation. In the figure $\phi_L(t)$ are blue and $\theta_L(t)$ are red.

maneuver. This method is inspired by skilled operators of cargo cranes. Consider a over-head single-axis translational crane, and a horizontal movement is desired. If the operator would simply push the button to move the crane and hold it in, a suspended load would start to swing. However, if the operator pushed the button once, to generate a step and initial swing, and then pushed again at the exact time when the load have zero swing angle, the resulting motion would cancel out the residual swing.

This method is popular in the literature, and the reader is referred to [9] for a thorough introduction to the method. By following the design procedure in [14], an Input Shape Filter $\mathcal{I}$, as depicted in Figure 7, is designed as

$$A_1 = 0.4948,\ A_2 = 0.5052, t_2 = 0.8392$$

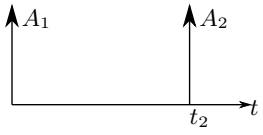

Fig. 7. Input shape filter $\mathcal{I}$, tuned after the frequency response of the pendulum-motion of the suspended load.

The resulting desired trajectory is obtained by the convolution of the shape filter:

$$\bar{\boldsymbol{\xi}} = \boldsymbol{\xi} * \mathcal{I} \tag{39}$$

so we now have collect the reference signals as $[\mathbf{r}(t), \dot{\mathbf{r}}(t), \ddot{\mathbf{r}}(t)] = \bar{\boldsymbol{\xi}}(t)$.

In this simulation, the multi-rotor will follow a box-like trajectory, as seen in the green line in Figure 9. All other parameters are identical to those in the previous section. In Figure 9, the the resulting path both with and without the input shape filter is presented, which illustrate the effectiveness of this procedure. Further, the tracking controller developed in this paper, is able to track the desired trajectory, as shown in Figure 11. Figure 10 shows the resulting load angles, with and without the input shape filter.

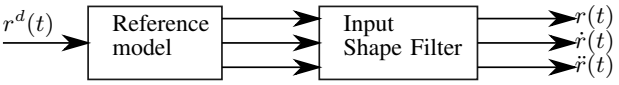

Fig. 8. Trajectory generation structure with an Input Shape filter and a third-order reference model.

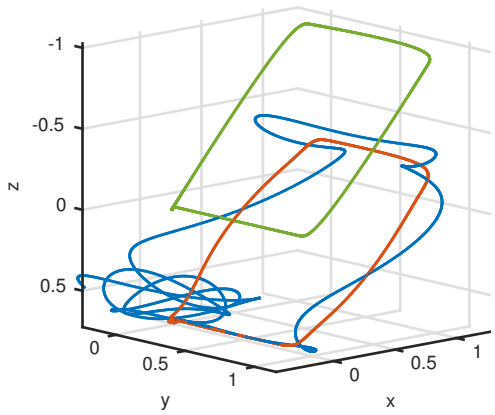

Fig. 9. The multi-rotor path (green), along with the suspended load position in Simulation two. The red path shows the load trajectory when an input shape-filter is enabled, the blue when it is disabled.

C. Discussions

In the foregoing sections, we demonstrated the controller on two simulation cases. In both cases, the trajectory controller presented in Theorem 1 tracked the desired trajectory perfectly. In the first simulation, we saw that the controller perfectly cancelled the effects of heavy load movements. In

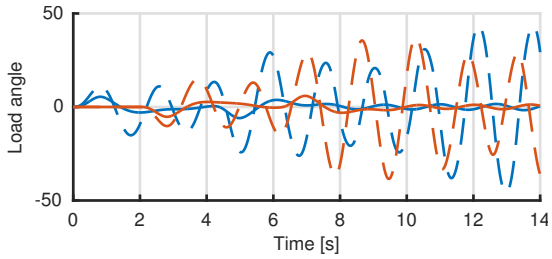

Fig. 10. Load angles with (solid) and without (dashed) input shaper

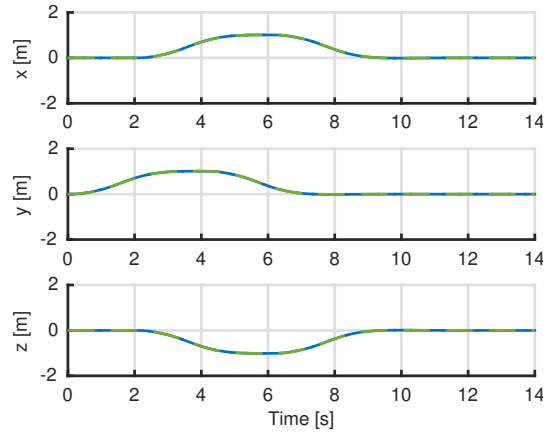

Fig. 11. Tracking results from simulation two. Multirotor position is given in solid blue, the reference in dashed green.

the second simulation, we illustrated how popular anti-swing techniques can be applied without any additional re-design of the controller. Active feedback-type swing-dampers can also be included in the design, for instance by applying a delayed feedback approach [15].

V. Conclusions

In this paper, we have studied trajectory control of a multirotor-type UAV with a suspended payload connected in the UAV COG. By assuming that the suspension wire is a rigid link, we developed mathematical models of the system using Kane's method. Further, we developed a perturbed model to avoid a representation singularity. The perturbation was done such that the models were equal for small load swing angles, and an infinitesimal term was added around the singularity $\theta_L = \pi/2$. Since the assumptions on the first model are unlikely to hold for such load angles, the additional effects of this perturbation is negligible in practice.

We proposed a theorem for trajectory control of the multirotor UAV with suspended payload, guaranteeing that the tracking error converges to zero. The equilibrium point was proven UGAS by Lyapunov analysis. We briefly showed how available techniques can be applied to generate trajectories for swing-free maneuvers.

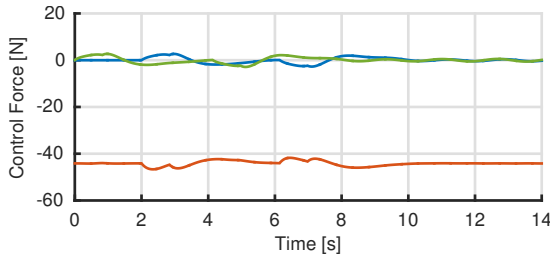

Fig. 12. Control inputs during simulation case two. Blue, green and red represents forces along x, y and z-axis, respectively.

References

[1] T. Lee, M. Leoky, and N. McClamroch, "Geometric tracking control of a quadrotor UAV on SE (3)," in *49th IEEE Conference on Decision and Control*, Atlanta, 2010, pp. 5420–5425.

[2] I. Palunko and R. Fierro, "Adaptive Control of a Quadrotor with Dynamic Changes in the Center of Gravity," in *18th IFAC World Congress, Italy*, 2011, pp. 2626–2631.

[3] T. Madani and A. Benallegue, "Backstepping Sliding Mode Control Applied to a Miniature Quadrotor Flying Robot," *IECON 2006 - 32nd Annual Conference on IEEE Industrial Electronics*, pp. 700–705, Nov. 2006.

[4] R. Mahony, V. Kumar, and P. Corke, "Modeling, Estimation, and Control of Quadrotor," *IEEE Robotics & Automation magazine*, vol. 19, no. 3, pp. 20–32, Sept. 2012.

[5] F. A. Goodarzi, D. Lee, and T. Lee, "Geometric Stabilization of Quadrotor UAV with a Payload Connected by Flexible Cable," in *American Control Conference (ACC)*. IEEE, Sept. 2014, pp. 4925–4930.

[6] K. Sreenath, N. Michael, and V. Kumar, "Trajectory generation and control of a quadrotor with a cable-suspended load - A differentially-flat hybrid system," *2013 IEEE International Conference on Robotics and Automation*, pp. 4888–4895, May 2013.

[7] M. Bernard and K. Kondak, "Generic slung load transportation system using small size helicopters," *2009 IEEE International Conference on Robotics and Automation*, pp. 3258–3264, May 2009.

[8] I. Maza, K. Kondak, M. Bernard, and A. Ollero, "Multi-UAV Cooperation and Control for Load Transportation and Deployment," *Journal of Intelligent and Robotic Systems*, vol. 57, no. 1-4, pp. 417–449, Aug. 2009.

[9] T. Singh and W. Singhose, "Input Shaping / Time Delay Control of Maneuvering Flexible Structures," in *American Control Conference, 2002. Proceedings of the 2002 (Volume:3)*, NY, USA, 2002, pp. 1717 – 1731 (3).

[10] M. Bernard and K. Kondak, "Autonomous transportation and deployment with aerial robots for search and rescue missions," *Journal of Field Robotics*, vol. 28, no. 6, pp. 914–931, 2011.

[11] O. Egeland and J. T. Gravdahl, *Modeling and Simulation for automatic control*. Marine Cybernetics, 2002.

[12] H. K. Khalil, *Nonlinear Systems*, 3rd ed. Prenctice Hall, 2002.

[13] T. Fossen, M. Breivik, and R. Skjetne, "Line-of-Sight Path Following of Underactuated Marine Craft," in *Proc. of the IFAC MCMC'03*. Girona, Spain: IFAC MCMC'03, 2003, pp. 1–6.

[14] M. Bisgaard, A. la Cour-Harbo, and J. Bendtsen, "Input Shaping for Helicopter Slung Load Swing Reduction," in *AIAA Guidance, Navigation and Control Conference and Exhibit*, Honolulu, Hawai, 2008.

[15] M. Bisgaard, A. Cour-harbo, and J. D. Bendtsen, "Swing Damping for Helicopter Slung Load Systems using Delayed Feedback," *Proceedings of AIAA Conference on Guidance, Navigation, and Control*, pp. 1–11, 2009.